Marine Structures 69 (2020) 102680

Contents lists available at ScienceDirect

Marine Structures

journal homepage: www.elsevier.com/locate/marstruc

Comparing different contour methods with response-based methods for extreme ship response analysis

Erik Vanem[a,*], Bingjie Guo[a], Emma Ross[b], Philip Jonathan[c,d]

[a] DNV GL Group Technology and Research, Høvik, Norway
[b] Shell Global Solutions, Amsterdam, the Netherlands
[c] Shell Research Ltd., London, United Kingdom
[d] Lancaster University, Department of Mathematics and Statistics, Lancaster, United Kingdom

ARTICLE INFO

Keywords:
Extreme ship response analysis
Marine structures
Environmental contours
Structural reliability
Response-based methods
Ocean environment
Environmental loads

ABSTRACT

Environmental contours are often applied in probabilistic structural reliability analysis to identify extreme environmental conditions that may give rise to extreme loads and responses. They facilitate approximate long term analysis of critical structural responses in situations where computationally heavy and time-consuming response calculations makes full long-term analysis infeasible. The environmental contour method identifies extreme environmental conditions that are expected to give rise to extreme structural response of marine structures. The extreme responses can then be estimated by performing response calculations for environmental conditions along the contours.

Response-based analysis is an alternative, where extreme value analysis is performed on the actual response rather than on the environmental conditions. For complex structures, this is often not practical due to computationally heavy response calculations. However, by establishing statistical emulators of the response, using machine learning techniques, one may obtain long time-series of the structural response and use this to estimate extreme responses.

In this paper, various contour methods will be compared to response-based estimation of extreme vertical bending moment for a tanker. A response emulator based on Gaussian processes regression with adaptive sampling has been established based on response calculations from a hydrodynamic model. Long time-series of sea-state parameters such as significant wave height and wave period are used to construct N-year environmental contours and the extreme N-year response is estimated from numerical calculations for identified sea states. At the same time, the response emulator is applied on the time series to provide long time-series of structural response, in this case vertical bending moment of a tanker. Extreme value analysis is then performed directly on the responses to estimate the N-year extreme response. The results from either method will then be compared, and it is possible to evaluate the accuracy of the environmental contour method in estimating the response. Moreover, different contour methods will be compared.

1. Introduction and background

Environmental contours are often used in long-term extreme response analysis of marine structures as a simple and approximate alternative to more computationally demanding full long-term analyses. One of the main advantages of environmental contours is

* Corresponding author.
E-mail address: Erik.Vanem@dnvgl.com (E. Vanem).

https://doi.org/10.1016/j.marstruc.2019.102680
Received 22 March 2019; Received in revised form 10 August 2019; Accepted 16 September 2019

that the structural response analysis is de-coupled from the environmental description, meaning that only a limited number of short term response calculations are needed for long-term analysis. That is, the environmental contours method identifies critical environmental conditions for which short term analysis is performed [1]. Response-based analysis is an alternative to contour-based methods, if the response is known or if a reasonable approximator for the response can be established at affordable computational cost.

Environmental contours were first proposed as equi-density lines [2], but currently contours based on the inverse first order reliability method (IFORM) are more widely used [3,4]. More recently, environmental contours based on direct Monte Carlo sampling have been proposed [5,6]. These contours have well-defined probabilistic properties, and will in some cases be quite different from the traditional IFORM-contours, see the comparison studies in Refs. [7,8] and also [9]. In particular, the direct sampling contours will by definition always enclose a convex set, whereas the IFORM contours will tend to follow the scatter of the data more closely. Other approached for environmental contours exist, see e.g. Refs. [10–17] or the recent review in Ref. [18].

In this paper various approaches to environmental contours will be used, and the results from an approximate long-term analysis using such contours will be compared to an approximate long-term analysis based on a statistical response emulator. Moreover, different modelling approaches for the long-term wave description will be explored, including an initial distribution approach and a conditional extremes modelling approach. A recent comparison study of response-based and contour-based methods was presented in Ref. [19]. Moreover, parts of the study presented herein was presented in Ref. [20]. In the following, a brief introduction to the different methods for constructing environmental contours will be given, as well as an introduction to Gaussian processes models which has been used for the response emulator.

1.1. Environmental contours

The direct sampling approach to environmental contours utilizes Monte Carlo sampling from a joint distribution of environmental parameters in order to draw contour lines corresponding to a target exceedance probability. That is, each segment of the environmental contour corresponds to a hyperplane with a specified exceedance probability, and under the assumption of a convex failure region this will represent an upper bound on the failure probability of a structure. The full recipe for calculating environmental contours with the direct sampling approach will not be repeated herein, but reference is made to previous publications [5,6,21]. In short, the environmental contours are calculated as follows (in the 2-dimensional case for bivariate variables (T, H); higher dimensional contours can be constructed in a similar way, see e.g. Ref. [22]): Let P_e be the target exceedance probability. The first step is to simulate a sufficiently large number of Monte Carlo samples from the joint distribution model. Then for any given angle $\theta \in [0,360)$, identify a straight line $\Pi(\theta)$ defined by an equation on the form $t\cos(\theta) + h\sin(\theta) = C(\theta)$, partitioning the sample space into two halfspaces $\Pi(\theta)^+$ and $\Pi(\theta)^-$ such that the fraction of sample points in $\Pi(\theta)^+$ is approximately equal to P_e. The resulting set $\mathscr{B}$ is then obtained by intersecting the sets $\Pi(\theta)^-$ for all $\theta \in [0,360)$, and constitute the environmental contours.

The IFORM approach to environmental contours is outlined in Refs. [3,4], and essentially finds the environmental contour by transforming a circle with radius corresponding to the target reliability level in standard normal space to the space of the environmental variables, in this case significant wave height and wave period. The resulting contour will describe the extreme wave climate based on exceedances probabilities in the standard normal space and is based on a linear approximation of the limit state function in that space. One difference between the direct sampling contours and the IFORM-based contours is that the direct sampling contour will always be convex, whereas the IFORM contour need not be, see also [7,8].

Two other contour methods are applied in this study based on the conditional extremes model, namely joint exceedance contours and isodensity contours. Joint exceedance contours are based on a definition proposed in Ref. [23]. In this study, isodensity contours are estimated from simulation under a conditional extremes model; further description is given in Section 2.2.

The calculation of environmental contours is based on a joint distribution describing the relevant metocean parameters, for example the significant wave-height H_s and peak wave-period T_p. The joint distribution is in turn normally based on some dataset. There are uncertainties related to the fitting of a joint distribution to data and the results strongly depend on the choice of parametric model [24] and other choices made during the fitting procedure [25]. Moreover, there is also an uncertainty related to the fact that the underlying metocean sample is of finite size [26]. These uncertainties will obviously be propagated to the environmental contours, and should be acknowledged when applying contour methods [27,28].

1.2. Gaussian processes regression

A stochastic process is a collection of random variables typically associated with a set of continuous indices such as space, time or any other input variables. A Gaussian process is a stochastic process where every realization of the process, that is, every finite collection of the random variables, have a multivariate normal (Gaussian) distribution, and it can be regarded as an infinite-dimensional generalization of the multivariate normal distribution.

The distribution of a set of multivariate normal random variables is fully specified by its mean vector $\boldsymbol{\mu}$, specifying the expected value of each random variable, and its covariance matrix $\boldsymbol{\Sigma}$, specifying the variances of each random variable as well as the covariance between any pair of random variables. The density of a collection of random variables $\boldsymbol{Y}^T = (Y_1, Y_2, ..., Y_k)$ which are multivariate normally distributed with mean vector $\boldsymbol{\mu}$ and covariance matrix $\boldsymbol{\Sigma}$ is

$$f(\boldsymbol{y}) = \frac{1}{\sqrt{(2\pi)^k |\boldsymbol{\Sigma}|}} e^{-\frac{1}{2}(\boldsymbol{y}-\boldsymbol{\mu})^T \boldsymbol{\Sigma}^{-1}(\boldsymbol{y}-\boldsymbol{\mu})}. \tag{1}$$

One important feature of the multivariate normal distribution is that if a set of random variables are jointly multivariate normally distributed, then the *marginal* distribution of any of the random variables will be Gaussian. Moreover, the conditional distribution of any of the random variables given the others will also be normal. In Gaussian processes, the mean vector is replaced by the mean function and the covariance matrix is replaced by a covariance function, which are typically continuous functions determining the process' behaviour over the input space. Having specified these functions, the Gaussian process is fully specified over the input space. For a homogeneous Gaussian process, the covariance function, $\kappa(\boldsymbol{x}, \boldsymbol{x}')$ will only depend on the distance between points in the input space, $d = |\boldsymbol{x} - \boldsymbol{x}'|$.

In Gaussian processes regression, the properties of Gaussian processes are exploited, and if a random process can be modelled as a Gaussian process, it may be used to predict the distribution at unobserved points in the input space. Such predictions will not only be point predictions, but it will provide the marginal distributions at unobserved points (which will be a marginal normal distribution) and hence also provide an estimate of the uncertainty. Given a set of observations from the Gaussian process, predictions may be the conditional distributions given the observed values. Typically, in Gaussian processes regression, the dependent variables $\boldsymbol{Y}$ are modelled as a Gaussian process over the space of the input variables, $\boldsymbol{X}$, and the training data set is used to estimate the mean- and covariance functions as well as to provide predictive distributions for unobserved points in input space.

Gaussian process regression utilizes the following general results of a partitioned multivariate normal vector: For

$$\begin{pmatrix} \boldsymbol{X}_1 \\ \boldsymbol{X}_2 \end{pmatrix} \sim MVN\left\{ \begin{pmatrix} \boldsymbol{\mu}_1 \\ \boldsymbol{\mu}_2 \end{pmatrix}, \begin{pmatrix} \boldsymbol{\Sigma}_{11} & \boldsymbol{\Sigma}_{12} \\ \boldsymbol{\Sigma}_{21} & \boldsymbol{\Sigma}_{22} \end{pmatrix} \right\}, \tag{2}$$

the conditional distribution of $\boldsymbol{X}_1$ given $\boldsymbol{X}_2$ is a multivariate normal distribution with mean and variance given by

$$\begin{aligned} E[\boldsymbol{X}_1|\boldsymbol{X}_2] &= \boldsymbol{\mu}_1 + \boldsymbol{\Sigma}_{12}\boldsymbol{\Sigma}_{22}^{-1}(\boldsymbol{X}_2 - \boldsymbol{\mu}_2) \\ Var[\boldsymbol{X}_1|\boldsymbol{X}_2] &= \boldsymbol{\Sigma}_{11} - \boldsymbol{\Sigma}_{12}\boldsymbol{\Sigma}_{22}^{-1}\boldsymbol{\Sigma}_{21} \end{aligned} \tag{3}$$

For a set of n training points $\boldsymbol{y} = \{y_1(\boldsymbol{x}_1), y_2(\boldsymbol{x}_2), ..., y_n(\boldsymbol{x}_n)\}$, the predictive distribution for another point $y_\star(\boldsymbol{x}_\star)$ can then be made based on the covariance matrices for the observed and predicted values. Letting

$$\begin{aligned} \boldsymbol{K} &= \begin{bmatrix} \kappa(\boldsymbol{x}_1, \boldsymbol{x}_1) & \kappa(\boldsymbol{x}_1, \boldsymbol{x}_2) & \cdots & \kappa(\boldsymbol{x}_1, \boldsymbol{x}_n) \\ \kappa(\boldsymbol{x}_2, \boldsymbol{x}_1) & \kappa(\boldsymbol{x}_2, \boldsymbol{x}_2) & \cdots & \kappa(\boldsymbol{x}_2, \boldsymbol{x}_n) \\ \vdots & \vdots & \ddots & \dots \\ \kappa(\boldsymbol{x}_n, \boldsymbol{x}_1) & \kappa(\boldsymbol{x}_n, \boldsymbol{x}_2) & \cdots & \kappa(\boldsymbol{x}_n, \boldsymbol{x}_n) \end{bmatrix} \\ \boldsymbol{K}_{\star\star} &= \kappa(\boldsymbol{x}_\star, \boldsymbol{x}_\star), \end{aligned} \tag{4}$$

the predictive distribution of $y_\star$ given the data $\boldsymbol{y}$ will then be (for simplicity, assuming a zero-mean process)

$$y_\star|\boldsymbol{y} \sim N(\boldsymbol{K}_\star \boldsymbol{K}^{-1}\boldsymbol{y}, \boldsymbol{K}_{\star\star} - \boldsymbol{K}^{-1}\boldsymbol{K}_\star^T). \tag{5}$$

In order to train a Gaussian process model, we need to specify the type of covariance function and in this study the radial basis kernel function is used. This kernel function has one hyper parameter, the inverse kernel width, h, and takes the following form:

$$\kappa(\boldsymbol{x}, \boldsymbol{x}') = \sigma^2 e^{-\frac{1}{2h^2}\left|\left|\boldsymbol{x}-\boldsymbol{x}'\right|\right|^2}. \tag{6}$$

This kernel is also sometimes referred to as the Gaussian or the squared exponential kernel. In addition, a nugget effect or variance may be included to account for noisy data, and this may typically be a constant value, for example on the form $c\delta(i, j)$ where $\delta(\cdot)$ denote the delta function and c is the noise variance. The modified kernel then takes the form

$$\kappa(\boldsymbol{x}, \boldsymbol{x}') = \sigma^2 e^{-\frac{1}{2h^2}\left|\left|\boldsymbol{x}-\boldsymbol{x}'\right|\right|^2} + c\delta(\boldsymbol{x}, \boldsymbol{x}'). \tag{7}$$

Estimation of the parameters σ^2 and c can be done by maximum likelihood or Bayesian methods [29].

2. Wave data description

A good wave climate description is needed in order to calculate ship responses in realistic sea states. In this study, non-linear numerical wave models have been used to simulate ocean waves given concurrent values of the sea state parameters significant wave height and spectral peak wave period, (H_S, T_P). Hence, a probabilistic description of the wave climate in terms of these variables are needed and the input to both numerical response calculations and construction of environmental contours are joint data for H_S and T_P. For the purpose of this study, wave climate data from numerical models have been used for one location in the North Atlantic Ocean. The data consist of 3 sets of 30-year time-series for the period January 1971 to December 2000 corresponding to three ensemble members from model runs (referred to as r2, r9 and r12 respectively), as described in Refs. [30,31]. The location of the data is 57.62° N, 20.28° W. It is assumed that the three model runs are three independent and equally likely realizations of the ocean wave climate at this location and these data will be utilized in this study. Hence, results will be presented for each of the subsets of 30-year data, as well as a combined dataset from all three ensembles. In the latter case, it is tacitly assumed that the combined data represents 90 years of wave climate data for a stationary wave climate. Scatterplots of the three datasets are presented in Fig. 1.

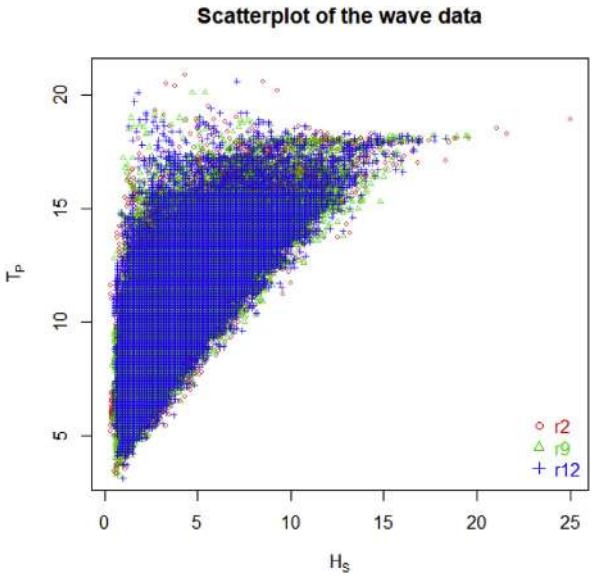

Fig. 1. Scatterplots of the wave climate data.

In this paper, two different approaches will be used to describe the underlying distribution of the wave climate based on the available data. The first uses all the data and fits a parametric joint distribution function to the data. The second approach uses peak-picking and fits a conditional extremes model to the jointly extreme data obtained in the peak-picking step. These models will be further outlined in the following.

2.1. A Weibull–log-normal model for sea state H_s, T_P, and estimated environmental contours

The datasets described in the previous section have been used to fit parametric distribution models for H_S and T_P in order to establish environmental contours for probabilistic reliability assessment. There are many alternative ways of fitting a parametric model to such data [24], and for this study a conditional model with a marginal 3-parameter Weibull distribution for H_S and a conditional log-normal distribution for T_P is assumed, see also [32], as follows:

$$f_{H_s}(h_s) = \frac{\beta}{\alpha}\left(\frac{h_s-\gamma}{\alpha}\right)^{\beta-1}\exp\left[-\left(\frac{h_s-\gamma}{\alpha}\right)^{\beta}\right], \tag{8}$$

$$f_{T_p|H_s}(t_p|h_s) = \frac{1}{\sigma(h_s)t_p\sqrt{2\pi}}\exp -\frac{(\ln t_p-\mu(h_s))^2}{2\sigma(h_s)^2}, \tag{9}$$

where

$$\mu = E\left(\ln T_p|H_S=h_S\right) = a_1 + a_2 h_s^{a_3}, \qquad \sigma = std\left(\ln T_p|H_S=h_S\right) = b_1 + b_2\, e^{b_3 h_s}. \tag{10}$$

The model parameters for the marginal distribution are fitted by minimizing the 2nd order Anderson Darling statistic. The parameters of the conditional model are fitted by calculating conditional means and standard deviations for binned data and then fitting functional forms to these binned values by least square fitting, as outlined in Ref. [8], see also [25].

The estimated model parameters are presented in Table 1, and the corresponding environmental contours for the 25-year conditions are shown in Fig. 2. The differences between the contours can be ascribed to sampling variability [26] and all contours are

Table 1
Distribution parameters estimated to the various datasets for the sea states.

	3-parameter Weibull (H_S)			Conditional log-normal (T_P)					
	(scale)	(shape)	(location)	(log-mean)			(log-std)		
	α	β	γ	a_1	a_2	a_3	b_1	b_2	b_3
r2	2.426	1.195	1.327	0.678	1.378	0.165	0.0150	0.193	−0.122
r9	2.630	1.253	1.120	1.565	0.513	0.339	0.0150	0.200	−0.129
r12	2.727	1.288	1.083	1.854	0.266	0.492	0.0150	0.228	−0.152
Combined data	2.609	1.251	1.165	1.203	0.871	0.231	0.0150	0.212	−0.139

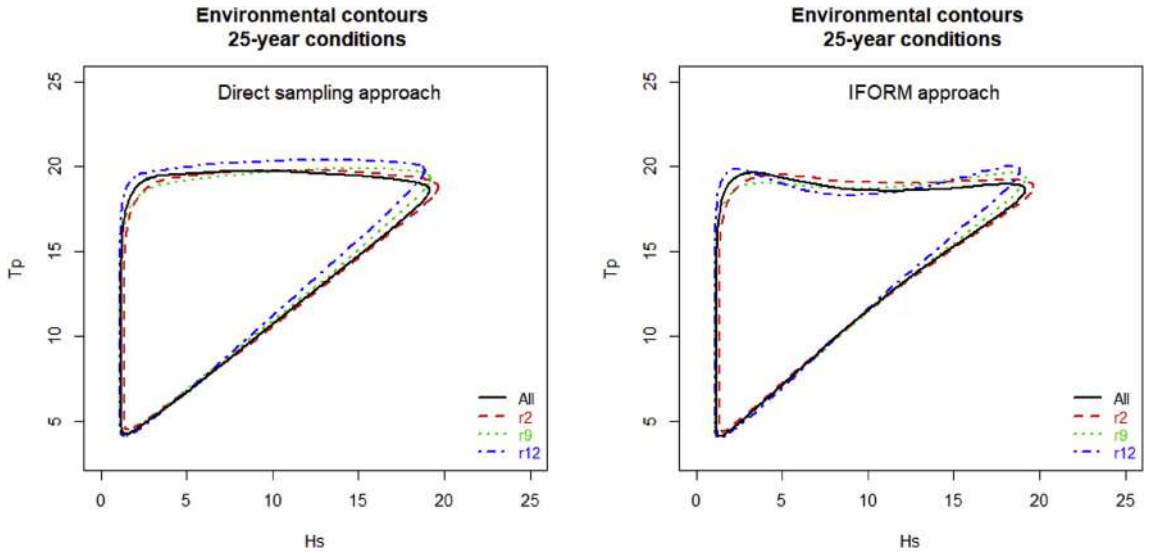

Fig. 2. Estimated environmental contours for the different datasets; Direct sampling approach (left) and IFORM approach (right).

assumed to represent an equally likely description of the 25-year extreme wave climate for the location under investigation. It is also observed that the contours based on the direct sampling approach and the IFORM describe similar extreme wave conditions, but there are some differences with respect to the shape of the contours. As expected, the direct sampling contours are convex and the IFORM contours are not.

2.2. A conditional extremes model for storm peak H_S, T_P, and associated environmental contours

We can use the output of numerical model runs for the ocean environment, or the output of emulators for the environment, or indeed direct observations of the environment to estimate conditional extremes models and hence environmental contours. Joint models and contours in this section are based on some sample of storm peak events of H_S and associated values of T_P. This sample is isolated from sea-state time-series using the procedure described by Ref. [33]. The conditional extremes model of [34], and its numerous extensions, provide a framework to estimate joint densities of H_S and T_P, and hence design contours. The approach is motivated by the asymptotic form for the limiting conditional behaviour of one variable, (Y_2 for definiteness here) given a large value y of a conditioning variable (Y_1), given by

$$Y_2|\{Y_1 = y\} = \alpha y + y^{\beta}(\mu + \sigma Z). \tag{11}$$

Parameters $\alpha \in [-1,1]$, $\beta \in (-\infty, 1]$, $\mu \in (-\infty, \infty)$ and $\sigma \in (0, \infty)$ are estimated from the data, together with a sample to represent the distribution of residual process Z. See Ref. [35] for details.

The conditional dependence of environmental variables may itself change as a function of over environmental covariates (such as wave direction or season). To apply the conditional extremes model to non-stationary data with dependence on one or more covariates, the sample is partitioned into a number of covariate bins, within which homogeneous extreme value characteristics are assumed. The model for covariate bin B then takes the form

$$Y_2|\{Y_1 = y, B\} = \alpha_B y + y^{\beta}(\mu + \sigma Z_B). \tag{12}$$

Estimates for the set $\{\alpha_B\}$ optimise predictive performance, assessed using cross-validation, using maximum roughness-penalised likelihood estimation. To estimate the conditional extremes model, variables Y_1 and Y_2 must be expressed on standard Laplace marginal scales. This is achieved by first fitting marginal gamma-generalised Pareto models for each of H_S and T_P as described in Ref. [36], followed by transformation (to Y_1, Y_2 respectively) using the probability integral transform. Parameters of marginal models are again constant within each covariate bin B, but vary between bins. In particular, the marginal shape parameter is assumed constant across all covariate bins, the marginal threshold parameter is assumed independent in different bins, and the marginal scale parameter is allowed to vary between bins, but a roughness penalty is introduced to ensure optimal smoothness between different covariate bins, as assessed by a cross-validation procedure. Simulation under the fitted conditional extremes model allows estimation of isodensity, joint exceedance and direct-sampling contours. Uncertainties in specification of marginal and conditional extremes thresholds, and marginal and conditional extremes parameter estimation, are propagated though to simulations using a bootstrapping scheme, again as described in Ref. [36]. In this study, covariates are wave direction and season, and the data are partitioned into seasonal-directional bins for the non-stationary analysis.

Inspection of directional-seasonal plots of the original samples suggested that a non-stationary analysis should be considered, see Fig. 3. Specification of covariate bin boundaries for the non-stationary analysis was based on inspection of the data, motivated by the

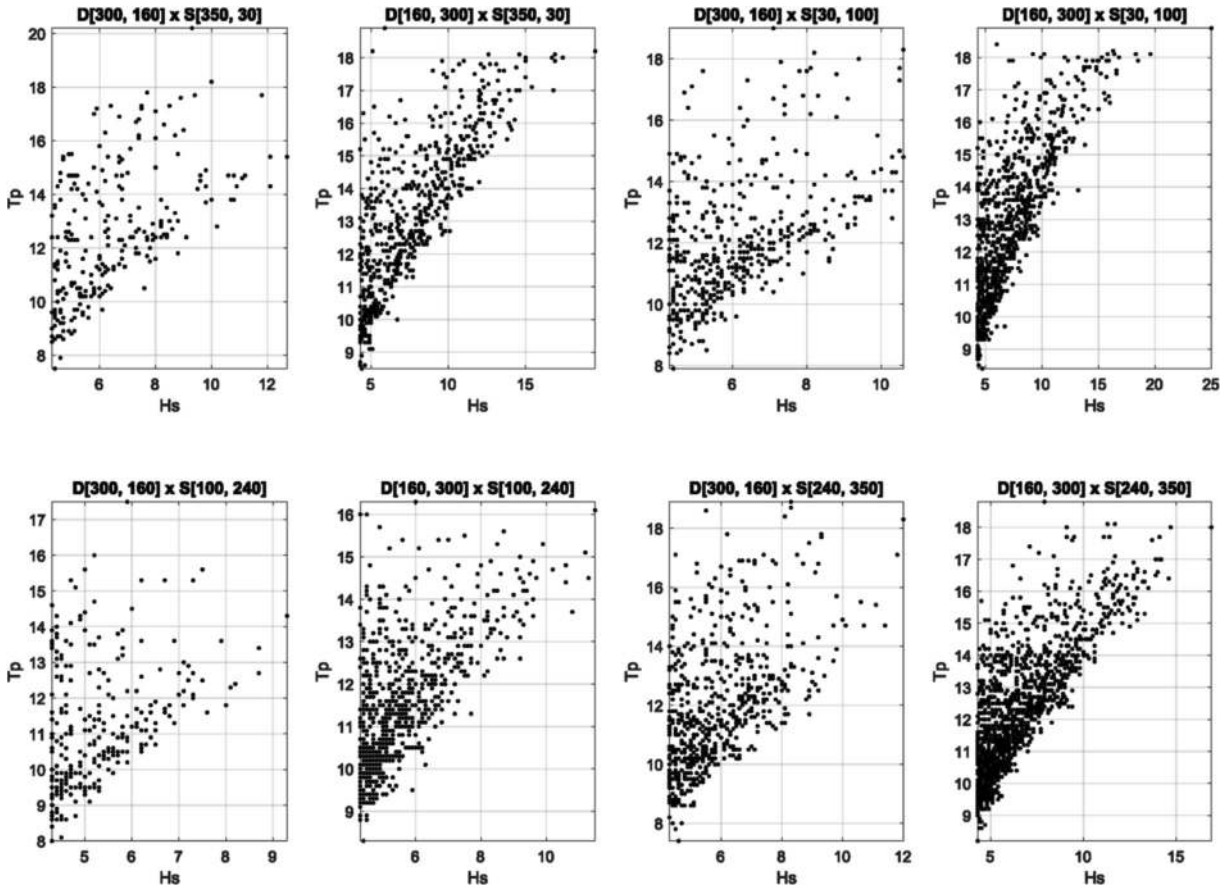

Fig. 3. Scatterplots of the original data samples for different directional-seasonal covariate bins.

requirement that each covariate bin appeared to show approximate homogeneity in diagnostic plots. For comparison, we also estimated a stationary model corresponding to allocating all observations in the sample to one covariate bin; it should be noted that diagnostic plots suggested that stationary models provided inferior fits to the samples. Fig. 4 illustrates isodensity, joint exceedance (Exc) and direct-sampling 25-year contours for the three datasets and for the combined dataset, from a stationary analysis. Omni-directional-seasonal contours from stationary and non-stationary analyses on the combined dataset are shown in Fig. 5. The main difference between stationary and non-stationary estimates is the fact that the non-stationary marginal model for H_S provides a larger estimate of the 100-year return value. Contours from the non-stationary analysis for different directional-seasonal bins are shown in Fig. 6. The variation in contour location across covariate bins is partly due to variation in rate of occurrence of events across bins. However, it is also clear that the joint density of H_S and T_P varies across covariate bins, suggesting that a non-stationary analysis is appropriate.

3. Case study: extreme vertical bending moment of an LNG tanker

The focus of this study is the 25-year extreme vertical bending moment of an LNG tanker. According to design rules for ships, design life is 25 years. The specified design life is the nominal period that the ship is assumed to be exposed to operating conditions [37] and it is therefore natural to consider the 25-year extreme response.

A full long-term approach to extreme response estimation can be formulated as an integral of short-term response distributions over the long-term distribution of governing sea-states variables, see e.g. Ref. [38]. However, evaluation of this integral is infeasible in most practical applications due to the computationally heavy calculations for the short-term response distributions for each sea state. Hence, approximate methods are often used that only requires short-term response calculations for a limited number of sea states. With the environmental contour method, it is implicitly assumed that the long-term variability of sea states dominates over the short-term variability of extreme response in a sea state, and the long-term extreme response analysis is based on the short-term extreme response in selected extreme sea states only. This is often referred to as a design sea state approach. With the response based approach used in this study, short-term extreme responses are calculated on a grid of important sea state variables, and an emulator is trained to estimate the extreme short-term responses for other combinations of the sea state variables. This will then provide a quick approximation of the maximum response in any sea state condition and can be used to generate long time-series of extreme short-

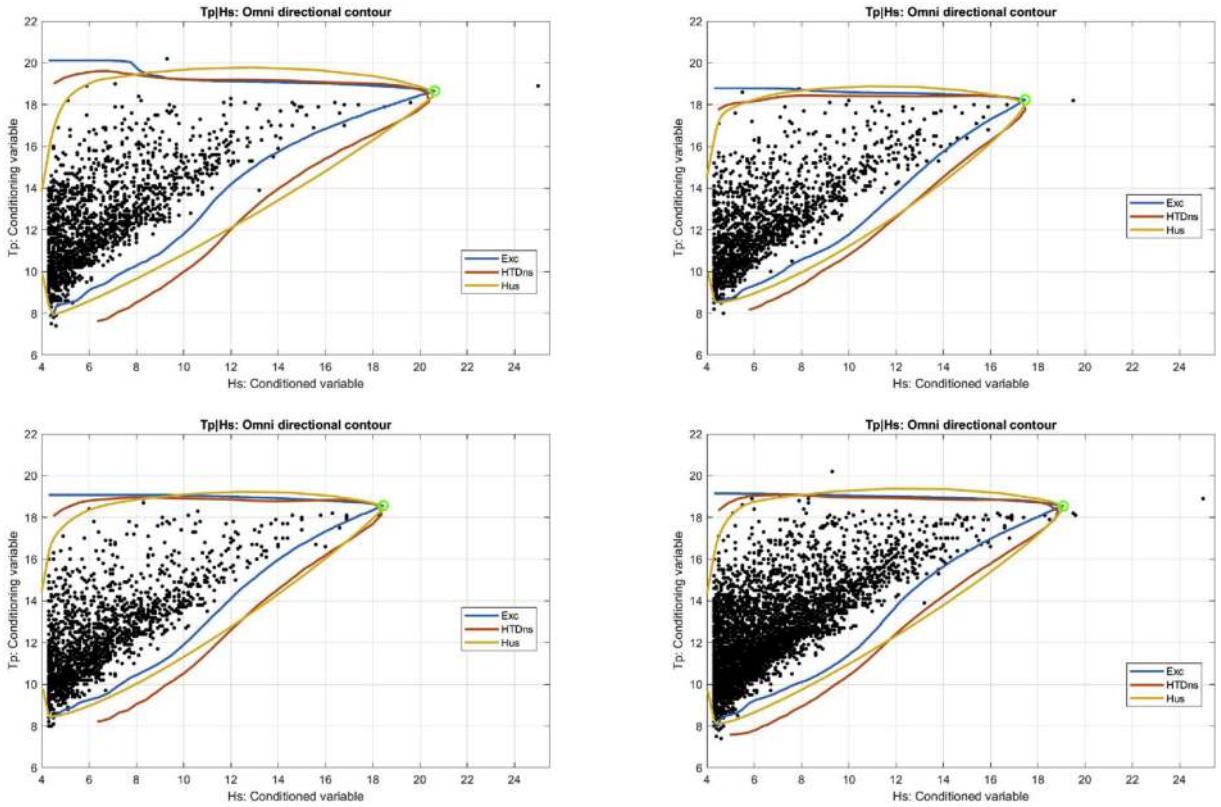

Fig. 4. Estimated environmental contours for the different datasets with the conditional extremes model; r2 data (top left), r9 data (top right), r12 data (bottom left) and the combined data (bottom right). *Exc* denotes joint exceedance contours, *HTDns* denotes isodensity contours and *Hus* denotes direct sampling contours, respectively. The circle corresponds to a lock-point used when calculating the contours.

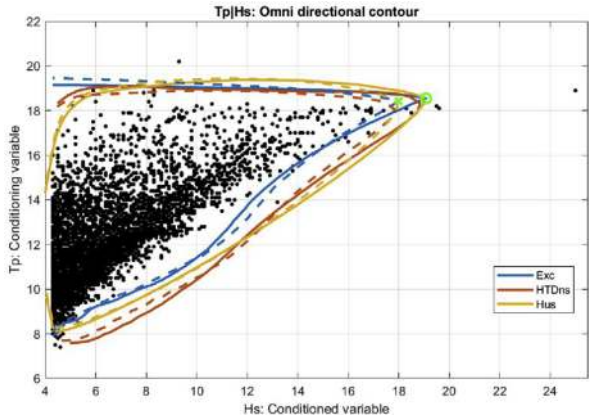

Fig. 5. Omni-directional contours based on non-stationary analysis (dashed lines) of the combined dataset compared to contours from stationary analysis (solid lines). *Exc* denotes joint exceedance contours, *HTDns* denotes isodensity contours and *Hus* denotes direct sampling contours, respectively. The green circle corresponds to a lock-point used when calculating the contours. (For interpretation of the references to colour in this figure legend, the reader is referred to the Web version of this article.)

term responses. In both cases, the method for calculation of extreme short-term response in a sea state is identical.

In order to make comparison of the environmental contour method and response-based analysis for extreme ship bending moment, a statistical emulator of the response for an LNG tanker is established using machine learning techniques, based on numerical simulation performed with Wasim combined with the nonlinear wave model UOSM [39,40]. We structure the presentation in this section as follows. The numerical simulations and its verification are given first. Then the response emulator is discussed in the subsequent sub-section.

One LNG tanker has been chosen for this study. The main parameters of the tanker are given in Table 2. Model tests on the LNG

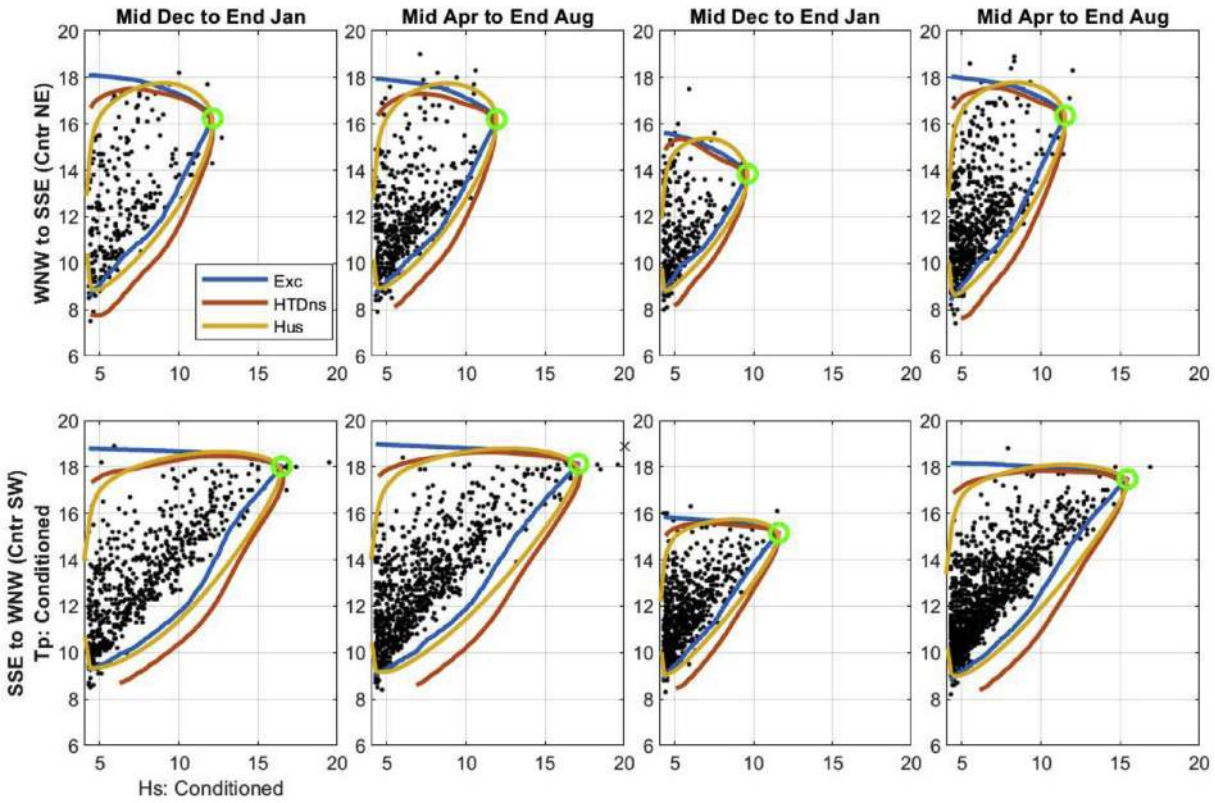

Fig. 6. Environmental contours for selected directional-seasonal bins based on non-stationary analysis of the combined dataset. *Exc* denotes joint exceedance contours, *HTDns* denotes isodensity contours and *Hus* denotes direct sampling contours, respectively. The green circle corresponds to a lock-point used when calculating the contours. (For interpretation of the references to colour in this figure legend, the reader is referred to the Web version of this article.)

Table 2
Main parameters of the LNG tanker.

	Unit	Full scale	Model scale
Scale	[−]	1	1/70
Length (Lpp)	[m]	186.90	2.670
Breadth (B)	[m]	30.38	0.434
Depth (D)	[m]	18.20	0.268
Draught (T)	[m]	8.40	0.120
Displacement (Δ)	[kg]	35 674 800	103.831
	[m]	94.8675	1.35525
	[m]	0	0
	[m]	8.26	0.118

tanker were performed in the sea-keeping basin of Technical University Berlin (TUB) at model scale 1:70 within the EC EXTREME SEAS project. A more detailed description of the model test can be found in Ref. [41].

3.1. Response calculations and verification

The 3-h extreme bending moment in a certain sea state is calculated with Wasim, with wave inputs from a nonlinear HOSM (Higher Order Spectral Method) wave model. For selected sea states, 3-h of ship bending moments have been simulated and a statistical distribution, $F(x)$ has been fitted to the local maxima by the method of moments. According to Ref. [42], the 3-parameter Weibull distribution is used, and this is also suggested by Ref. [43] for the short term hull girder response of ships. Having fitted the 3-parameter Weibull distribution to the short-term responses, and based on the number of local maxima N in the 3-h short-term responses, the distribution of the extreme maximum can be found from highest-order statistics as $F_e(x) = F(x)^N$. The characteristic extreme value, x_c, for vertical bending moment within the sea state is then calculated as the mode of the extreme value distribution by the following expression (assuming a 3-parameter Weibull distribution with location parameter γ, scale parameter α and shape

parameter β [42])

$$x_c = \gamma + \alpha(\ln N)^{\frac{1}{\beta}}. \tag{13}$$

WASIM solves the 3D radiation/diffraction problem using the Rankine panel method. The nonlinear Froude-Krylov force and hydrostatic force can be added to account partly for nonlinear effects. The HOSM code used in this study is internally developed DNV GL HOSM, which implements the HOSM methods presented in Ref. [40]. It also provides the full calculation of all water particle kinematics using the H2-operator method described in Ref. [44]. The HOSM code provides a consistent nonlinear calculation of the water particle kinematics to the given order M. In this study the nonlinear order was chosen as $M = 5$, which includes the most important nonlinear effects, including bound waves up to fifth order.

The numerical simulations with the 3D panel method and HOSM wave model were verified with model test as reported in Ref. [45]. The numerical simulation in linear waves were performed to verify the mesh and setting of the numerical model. The waves from the HOSM model and linear wave model are compared with model test to verify the HOSM wave model. The comparisons show that the HOSM model agrees better with model test than linear simulation. However, the HOSM model gives more extreme crests than experiments in some cases. The comparisons of ship bending moment of the LNG tanker from different numerical simulations with model tests show that nonlinear 3D panel method with the HOSM wave model slightly overestimates the ship hogging moment and gives the best prediction for the ship sagging moment. It was argued that the overestimation on wave crest by the HOSM model could be partly due to the fact that HOSM simulations are run without a wave breaking model. In this study, HOSM with a breaking model is adopted for wave simulation.

The verification of HOSM with a breaking model is performed in one irregular wave with $T_P = 12s$, $H_S = 9.7m$ and a peak enhancement factor for the JONSWAP wave spectrum $\gamma = 6$, as shown in Fig. 7. The comparison is performed in full scale. *Crest-HOSM* and *Trough-HOSM* give the exceedance probability of wave crest and trough from the HOSM wave model without any breaking model. *Crest-HOSM-BR* and *Trough-HOSM-BR* are wave results from the HOSM wave model with breaking. *Crest-LI* and *Trough-Li* gives the results from linear wave model and *Crest-exp* and *Trough-exp* refers to results from the model tests. The comparison confirms that the HOSM wave model can give better wave estimation than a linear wave model, especially for wave crests. The inclusion of a breaking model can improve the numerical results in the upper tail of the distribution.

The different numerical calculations of ship bending moments in the selected irregular sea state are compared in Fig. 8 to verify the numerical model adopted in this study. *xx-LI-LI* are results from pure simulation, where both the 3D panel program and the wave model are linear. *xx-HOSM* and *xx-HOSM-BR* represent the results from partly nonlinear 3D panel program with the HOSM wave model without and with a breaking model, respectively. *xx-Exp* denotes results from model tests. The results indicate that linear simulations tend to underestimate the ship sagging moment. The comparison also show that the breaking model can improve the accuracy, particularly for large bending moments. Thus, the partly nonlinear 3D panel program and the HOSM wave model with a breaking model are used to establish the response emulator outlined in the next section.

3.2. Response emulator

In order to perform response-based analysis, a method for efficiently approximating the response is needed and in this study a response emulator is established using Gaussian processes regression. 3-hours extreme bending moments are calculated for selected sea states, and these are used to train a Gaussian processes regression model, with bending moment as the target variable and (T_P, H_S)-values as explanatory variables. In this study, the Gaussian processes regression model uses a constant kernel combined with a radial basis function kernel. A nugget effect is included to account for the sampling variability of training samples due to the limited duration of simulation.

All the selected sea states are simulated with HOSM with the breaking model, using a JONSWAP wave spectrum and assuming

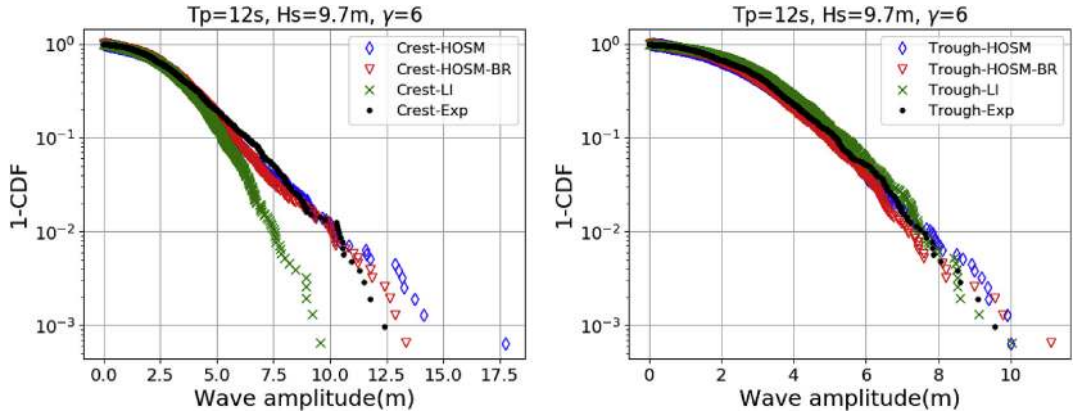

Fig. 7. Comparison of simulated wave data and model tests for a selected irregular sea state with $T_P = 12s$, $H_S = 9.7m$ and $\gamma = 6$; Wave crest (top) and wave trough (bottom).

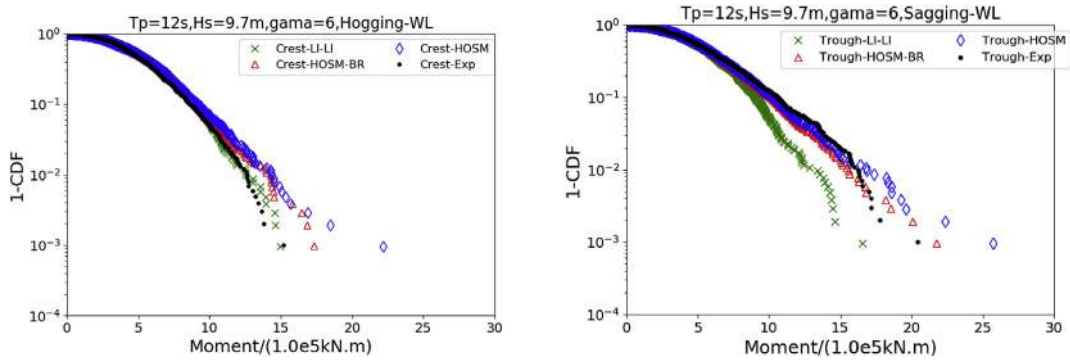

Fig. 8. Comparison of mid-ship bending moment at waterline in irregular sea with $T_P = 12s$, $H_S = 9.7m$ and $\gamma = 6$; Hoggind (top) and Sagging (bottom).

infinite water depth. The numerical simulations with the improved 3D panel method are performed for 3 h in full scale. The results are affected by sampling variability due to limited duration of the simulations. Thus, the local peak values of ship bending moments are fitted with the two-parameter Weibull distribution using the method of moments. Finally, the 3-h characteristic extreme value is estimated from the fitted Weibull distribution.

Nonlinear simulations are performed to calculate 3-h characteristic extreme value of ship bending moment, capturing the asymmetry of ship hogging and sagging response. Thus, the emulator is established for ship hogging and sagging separately. The applicability of Gaussian processes regression is verified by choosing some sea states to estimate 3-h characteristic extreme value of ship sagging and hogging moment with the 3D panel method for training the emulator and some sea states chosen for testing the emulator predictions. These selected sea states are illustrated in Fig. 9.

The fitted emulators for 3-h extreme hogging and sagging are shown in Fig. 10. This shows the predicted responses (mean values) for different variations of H_S and T_P, including 95% uncertainty bands. The training data are also indicated in the plots. These plots indicate that the Gaussian processes models capture the response surface quite well based on the training data.

Fig. 11 compares emulator predictions with numerical results for hogging and sagging, respectively, in the test data. The calculated bending moments (*true*) from the improved 3D panel method is compared to predictions from the Gaussian processes model (*pred*). This illustrates that the emulator performs well and can predict responses for sea states not included in the training data. The differences between the predicted and the calculated responses are larger in steep sea states compared to less steep sea states. This is presumably due to the fact that the effect of sampling variability is larger in steeper wave conditions.

There are some small waves with T_P less than 6s in the wave data (see Fig. 1). The bending moments will be very small for such conditions and will not be relevant for the 25-year extreme value. Moreover, linear simulations can give reasonable results for most of these wave conditions. In order to save computation cost, nonlinear simulations have not been carried out in this area and the emulator is therefore not extended to this area. However, linear calculations are utilized for these sea states in the response-based analysis.

4. Extreme response estimation

Having established a reasonable response emulator for the hogging and sagging bending moments, one may apply this to the complete time-series of environmental conditions and obtain equally long time-series of the structural response. Hence, 3 separate 30-

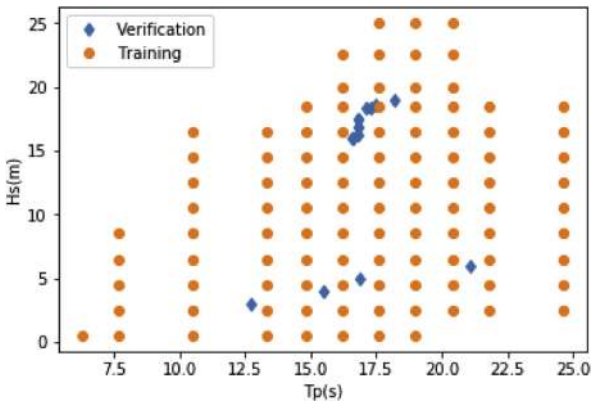

Fig. 9. Sea states selected for training and testing the response emulator.

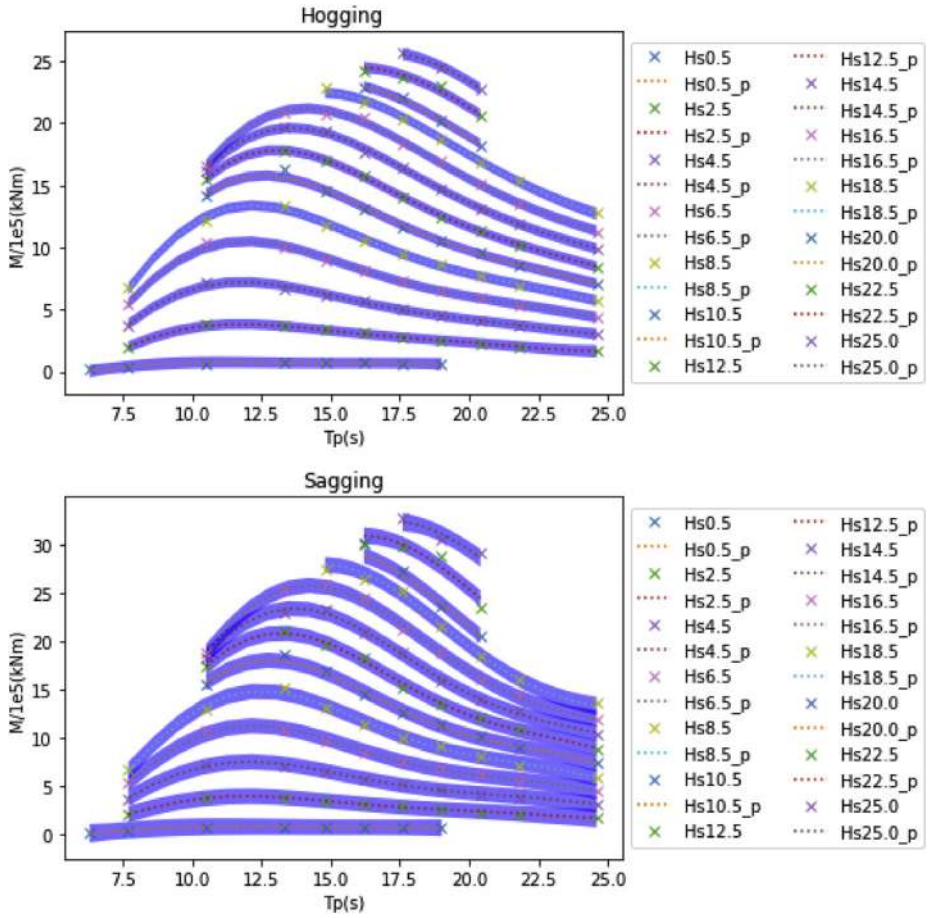

Fig. 10. Response surfaces as predicted by the Gaussian processes emulators; hogging (top) and sagging (bottom). The crosses denote the training data.

year time series of hogging and sagging responses are obtained and extreme value analysis can be done on each of them in order to estimate the 25-year response from the time series. In addition, the response emulator can be used for all points along the various environmental contours in order to estimate the contour-based 25-year responses.

4.1. Response based analysis

The emulator provides long time-series of structural responses for hogging and sagging bending moment which may be used to estimate 25-year extreme responses. There are different ways of estimating extremes from a long time-series and in this study the 25-year response is estimated in three ways. First, the empirical quantile can be found directly since the time series are longer than the target return period. For example, the 25-year extreme can simply be estimated as the $1 - 1/(25 \times 365.25 \times 8) \approx 0.9999863$-quantile from the empirical distribution. Secondly, a parametric distribution is fitted to all the response data, and the quantile according to the parametric model is calculated. It turns out that a 3-parameter Weibull distribution fits the data quite well, as illustrated by the QQ-plots in Fig. 12 for all the subsets of response data. Hence, quantiles from fitted 3-parameter Weibull distributions are used as alternative estimates of the 25-year response, where the fitting is done by minimizing the 2nd order Anderson Darling statistic. Finally, the block maximum approach is used on annual maxima data from the response time-series to obtain yet other estimates of the 25-year response directly from the emulated response time-series. Both the full GEV model and the reduced Gumbel model are fitted to annual maxima by maximum likelihood to provide yet other point estimates of the 25-year responses. It is acknowledged that other methods exist for extreme value analysis, and that there are considerable uncertainties associated with this. However, the uncertainties will decrease as the amount of data increases, and estimates will also be extracted from the combined dataset corresponding to 90 years of data. This study only considers point estimates of the extreme response, but confidence bounds could easily be found from bootstrapping.

The point estimates for 25 year hogging and sagging bending moments obtained from the response-based analysis are presented in Table 3. From these results, it is observed that there are considerable uncertainties due to sampling variability (different datasets) and different methods for extreme value extraction. Relative differences of up to 14% and 17% are seen for hogging and sagging

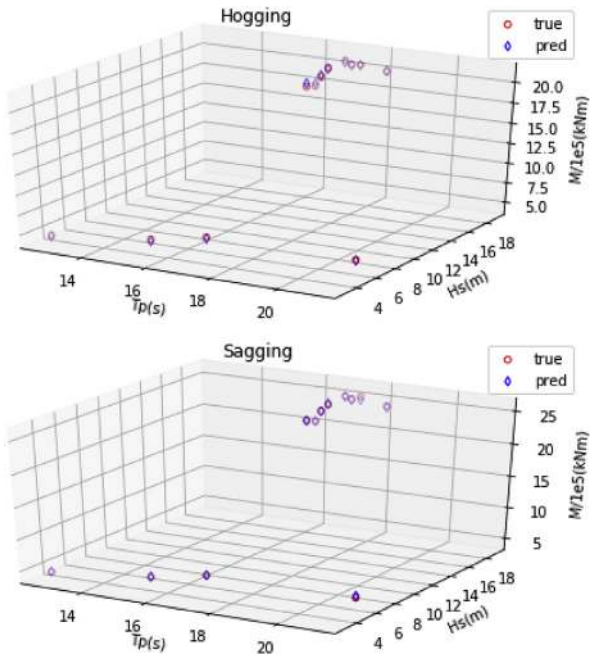

Fig. 11. Comparing emulator predictions on the test data; hogging (top) and sagging (bottom).

responses, respectively, for the different datasets, where the largest differences are for the empirical estimates. Comparing the various methods for the individual datasets, the relative differences are up to almost 15% and 18% for hogging and sagging, respectively, and the largest differences are found for the r9 dataset. Surprisingly, the relative differences across methods are somewhat larger for the combined dataset compared to the r2 dataset.

One may also check QQ-plots for the GEV and Gumbel fits to the annual maximum data, and this is shown in Figs. 13–14. It can be observed that the full GEV model appear to fit better than the reduced Gumbel model, and indeed, Wald tests indicate that the Gumbel model (with $\xi = 0$) would be rejected in all cases except for the hogging response for the combined dataset.

4.2. Extreme response analysis from the environmental contour method with initial distribution approach

By applying the environmental contour method, one may obtain estimates of the 25-year responses from only a few short-term analyses by running response calculations for sea state conditions described by the environmental contour only. In this study, environmental contours have been calculated as described above, and the response emulator has been utilized to get the associated responses. The 25-year response is then simply taken as the maximum response along the contours. With the calculated environmental contours shown in Fig. 2, the contour-based estimates of the 25-year responses in Table 4 are obtained.

It is observed that for all the datasets, the estimates obtained by the contour-method are comparable to the estimates from the response-based analysis. Indeed, except for the responses with the r12 dataset, the contour-based estimate lies within the range of values obtained by the different methods for response-based extreme value analysis. The relative differences (absolute value) between the various response-based estimates and the contour-based estimates range between 0.5% and 16% for the hogging response and between 0.9% and 20% for the sagging responses with the direct sampling contours and between 0.1% and 17% for the hogging response and between 0.8% and 22% for the sagging response with IFORM-based contours. The largest differences are in most cases for the estimates based on the Weibull fit to the response time-series, which also tend to be large compared to the other response-based estimates. It is also interesting to observe that the differences between the methods tend to be smaller for the combined dataset, indicating the importance of sampling variability in extreme response estimation. Hence, environmental contours have been demonstrated to give reasonable, approximate return values of extreme bending moment in this case study.

4.3. Extreme response analysis from the environmental contour method with a conditional extremes model

The conditional extremes model [34,46] introduced in section 2.2 was also applied to the wave climate data, and different contour methods have been applied to the results from this model. The resulting estimates of the 25-year extreme responses are presented in Table 5.

Both stationary and non-stationary analysis with respect to covariates were considered. A non-stationary analysis was performed for the combined dataset, where covariate effects due to varying direction (wind direction) and season were included in the model [47]. This results in different environmental contours for different seasonal-directional bins, which could again be combined to yield omni-seasonal-directional contours with the different contour methods (see Figs. 6 and 5). The 25-year extreme responses

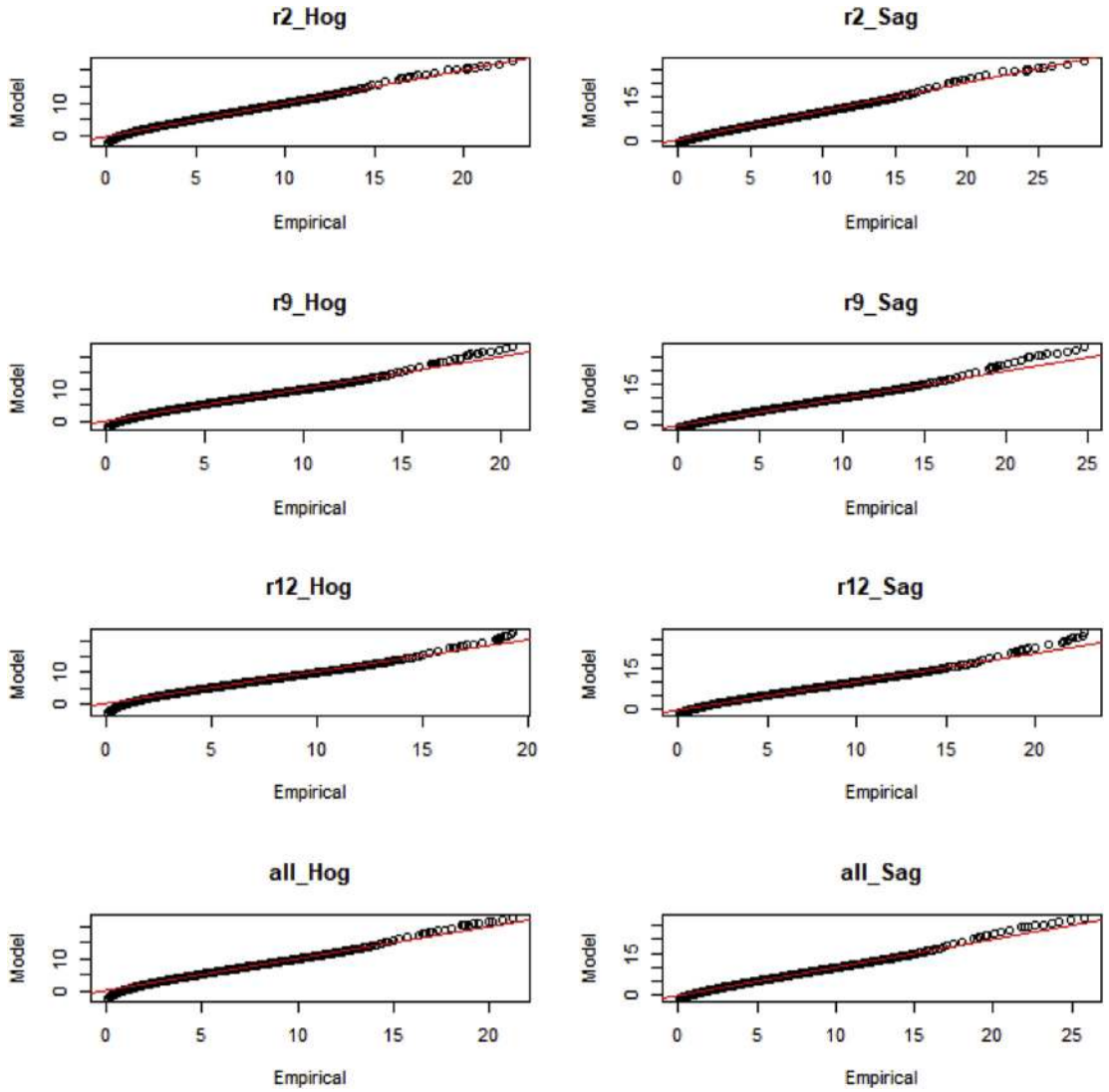

Fig. 12. QQ-plots for the 3-parameter Weibull distribution for the different datasets; hogging (left) and sagging (right).

Table 3
Estimated 25-year responses from response-based extreme value analysis (in 100 MNm).

Dataset	Empirical	Weibull	GEV	Gumbel
Hogging				
r2	22.382	22.168	21.498	20.534
r9	20.538	22.874	19.495	19.931
r12	19.227	22.234	19.320	19.892
Combined data	20.895	22.364	20.214	20.215
Sagging				
r2	27.519	27.049	26.191	24.324
r9	24.663	28.092	23.122	23.538
r12	22.698	27.292	22.850	23.342
Combined data	25.347	27.371	24.124	23.875

corresponding to the omni-directional-seasonal contours are included in Table 5.

It is found that the various contour methods applied together with the conditional extremes model compare reasonably well. However, the joint exceedance contours are found to give generally lower extreme responses than the other contour methods. Comparing the results from an initial distribution approach and the conditional extremes approach, it is also found that the results are comparable, and that the variability in the results are dominated by sampling variability. Indeed, dataset r2 yields higher extreme

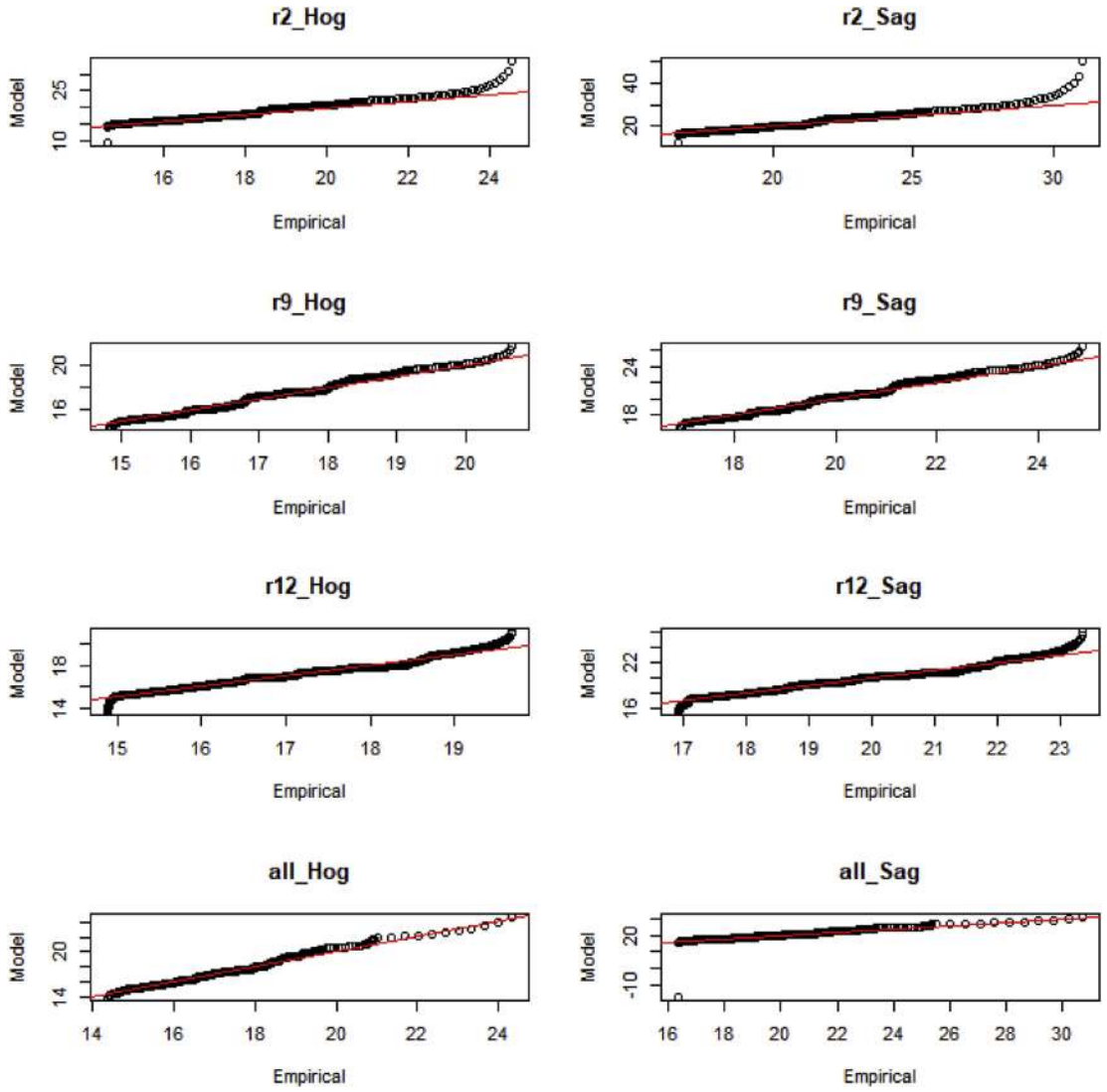

Fig. 13. QQ-plots for the GEV model fitted to annual maxima; hogging (left) and sagging (right).

response estimates regardless of contour method. This concurs with the response-based estimates, apart from those based on a Weibull fit to all response data. In summary, contours based on the conditional extremes model have also been demonstrated to give reasonable results. A further interesting observation is that the stationary analysis seems to give consistently lower estimates of the 25-year extreme response compared to the stationary analysis.

5. Discussion

5.1. Conditions giving rise to extreme response

Having estimated the 25-year extreme hogging and sagging bending moment using both response-based and contour-based methods, one may also look at which environmental conditions gave rise to the extreme responses by looking at the associated (H_S, T_P) values for the extreme responses. This is summarized in Table 6. For the response-based analysis, the associated sea-state conditions that give rise to the extreme responses are based on the empirical quantile estimates and the conditions corresponding to the largest response lower than the quantile and the smallest response greater than the empirical 25-year response in the dataset are reported in the table.

The response-based approach tends to identify more severe sea state conditions associated with the 25-year response compared to contour-based methods. This may be due to the fact that such events occur in the tail of the probability distributions where there are very few observations. However, the environmental contour method constructs a contour that also includes un-observed combinations of the environmental variables, whereas the response-based approach calculates the responses only for actually observed sea

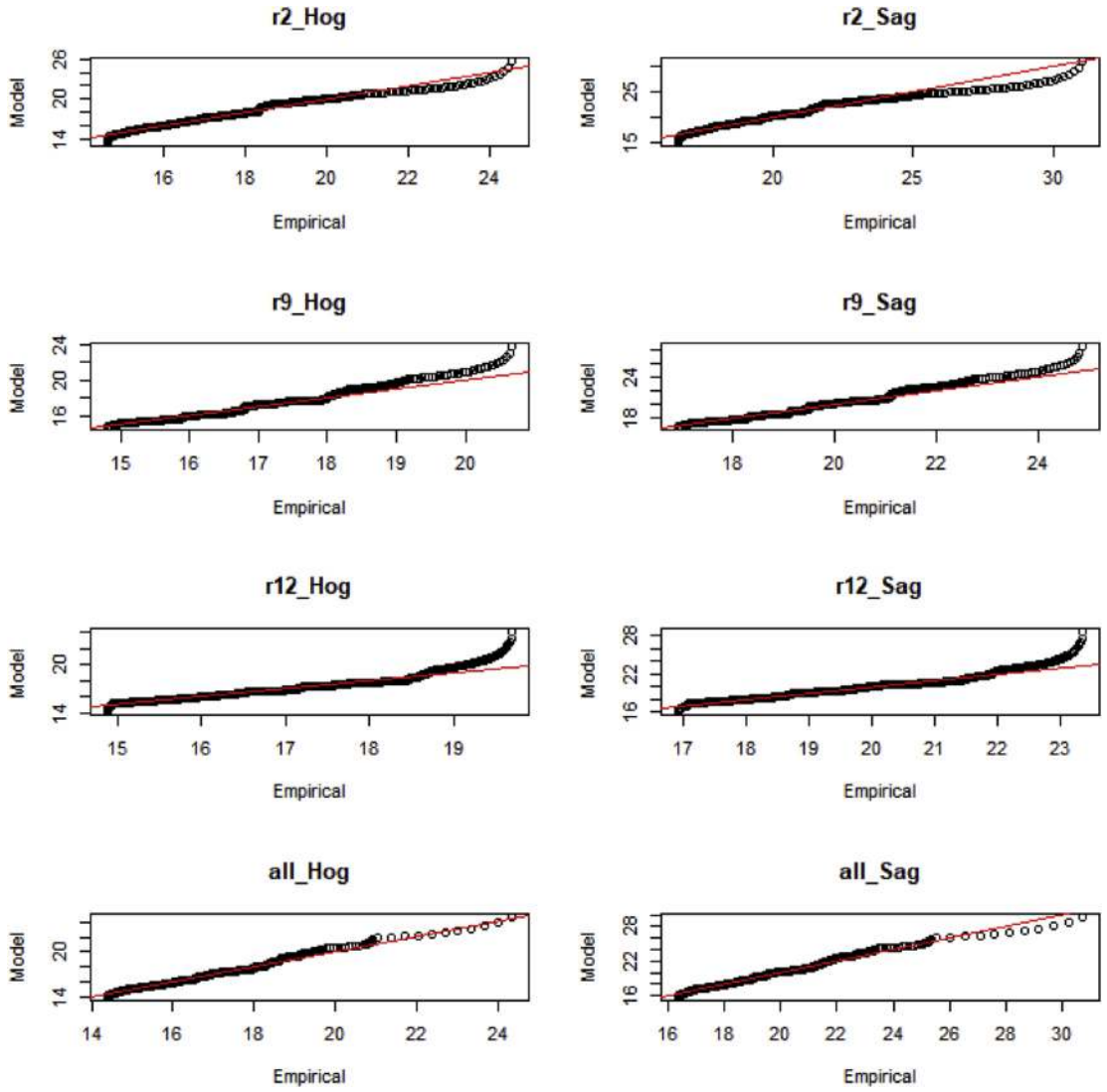

Fig. 14. QQ-plots for the Gumbel model fitted to annual maxima; hogging (left) and sagging (right).

state parameters. Hence, some combinations of environmental variables lying on the contour may not have been actually observed, and one may need to explore further out in the variable space to find the extreme responses. Notwithstanding this, from Tables 3–5 it is seen that the empirical response-based return value estimates are slightly higher than the contour-based estimates, and this correspond to more severe sea state conditions, as seen in Table 6. This is illustrated in the sagging case in Fig. 15, where the associated sea state conditions for the estimated extreme sagging response is illustrated (contour-results are shown for the initial distribution approach only). As can be seen, the contour-based estimates lie exactly on the environmental contours, whereas the sea states corresponding to the response-based estimates all lie outside the contours. The largest difference is observed for r2 scenario, whereas for r12, the lower response-based estimate coincides with the contour-based estimated conditions from the direct sampling contours. It may seem strange that the 25-year response can be generated by a sea state with a much higher return period than 25 years, and this is probably an effect of the bivariate distribution function fitted to the wave data and used for constructing the environmental contours.

5.2. Emulator response vs. numerical calculations for identified extreme conditions

Both the response-based and the contour based extreme responses were estimated by the response emulator. In order to investigate how good an approximator this emulator is to the extreme responses, the responses corresponding to sea states along the environmental contours that give rise to the extreme responses are also calculated by the hydrodynamical model and compared to the results from the emulator. The calculated responses from the emulator and the hydrodynamic model for these selected (H_S, T_P)-pairs are shown in Table 7.

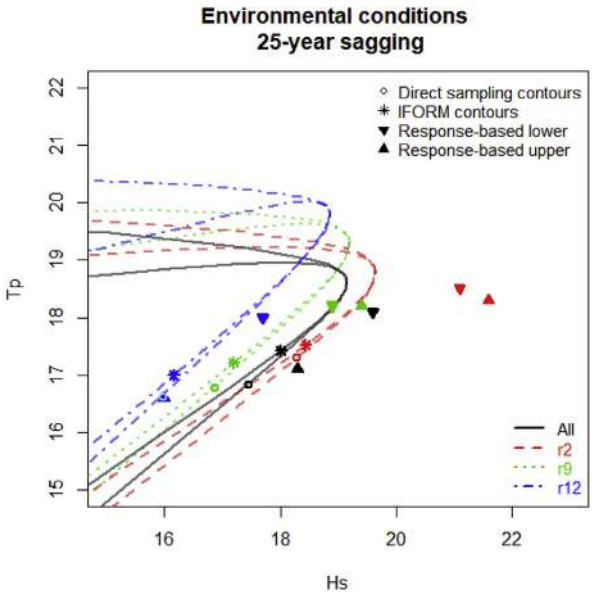

Fig. 15. Sea states associated with extreme sagging responses.

Table 4
Estimated 25-year responses from contour-based analyses with initial distribution approach (in 100 MNm).

	Direct sampling contours		IFORM contours	
	Hogging	Sagging	Hogging	Sagging
r2	20.643	24.992	20.549	24.786
r9	19.834	23.728	19.697	23.468
r12	19.145	22.652	18.898	22.248
Combined data	20.365	24.578	20.253	24.329

Table 5
Estimated 25-year responses from contour-based analyses with conditional extremes model (in 100 MNm).

	Direct sampling contours		Joint exceedance contours		Isodensity contours	
	Hogging	Sagging	Hogging	Sagging	Hogging	Sagging
r2	21.53	26.42	21.23	25.61	21.65	26.57
r9	19.62	23.41	18.71	21.80	19.59	23.33
r12	19.81	23.71	19.27	22.57	19.93	23.80
Combined data	20.55	24.88	19.89	23.55	20.44	24.66
Combined data; nonstationary analysis	20.03	24.05	18.99	22.23	19.76	23.60

It is observed that the emulator is a good approximator for the output from the hydrodynamical model, with relative differences less than 2% in all cases. This is negligible compared to the relative differences between the different results from various extreme value analysis methods on the emulated responses. Hence, the extra uncertainty due to the use of a response emulator is not significant in this case.

5.3. Modelling sea states vs. storm peaks

There is some debate within the user community regarding the relative merits of using observations of the environmental variables for serially-dependent sea states, compared with near-independent storm peak characteristics. Given that the rates of occurrence of events are taken into account, both can provide useful estimates of joint models for the environment and hence environmental contours. The advantage of using sea state data is that sample size is large, potentially allowing a more detailed description of the joint distribution of environmental parameters to be estimated. However, because sea state data is serially-correlated, naive estimates of uncertainties for model parameters and inferences under the model will be too small, but can be corrected (for example, using sandwich estimators or bootstrap resampling).

Table 6
Conditions giving rise to the 25-year responses from contour-based and response-based analyses; (H_S, T_P).

	r2	r9	r12	all
Hogging				
Response-based	(21.1, 18.5) - (21.6, 18.3)	(18.9, 18.2) - (19.4, 18.2)	(16.0–16.6) - (17.7, 18.0)	(18.3, 17.1) - (19.6, 18.1)
Initial distribution approach:				
Direct sampling contours	(18.54, 17.51)	(16.86, 16.79)	(16.22, 16.83)	(17.45, 16.83)
IFORM contours	(18.80, 17.80)	(17.65, 17.59)	(16.46, 17.25)	(18.35, 17.69)
Conditional extremes approach:				
Direct sampling contours	(19.54, 17.52)	(15.95, 16.12)	(16.69, 16.65)	(17.48, 16.68)
Non-stationary:				(16.39, 16.14)
Joint exceedance contours	(20.63, 18.65)	(17.46, 18.24)	(18.44, 18.56)	(19.08, 18.55)
Non-stationary:				(17.99, 18.43)
Isodensity contours	(19.88, 17.69)	(16.87, 17.02)	(18.00, 17.68)	(18.35, 17.52)
Non-stationary:				(17.13, 17.10)
Sagging				
Response-based	(21.1, 18.5) - (21.6, 18.3)	(18.9, 18.2) - (19.4, 18.2)	(17.7–18.0) - (16.0, 16.6)	(19.6, 18.1) - (18.3, 17.1)
Initial distribution approach:				
Direct sampling contours	(18.29, 17.30)	(16.86, 16.79)	(15.98, 16.62)	(17.45, 16.83)
IFORM contours	(18.44, 17.52)	(17.19, 17.22)	(16.16, 17.00)	(18.01, 17.42)
Conditional extremes approach:				
Direct sampling contours	(19.19, 17.25)	(15.95, 16.12)	(16.48, 16.45)	(17.48, 16.68)
Non-stationary:				(16.39, 16.14)
Joint exceedance contours	(20.63, 18.65)	(17.33, 18.14)	(18.44, 18.56)	(19.08, 18.55)
Non-stationary:				(17.71, 18.21)
Isodensity contours	(19.88, 17.69)	(16.86, 17.01)	(17.87, 17.58)	(17.85, 17.13)
Non-stationary:				(17.13, 17.10)

Table 7
Comparing response emulator with numerical model for selected sea states.

(H_S, T_P)	Numerical model	Emulator	Relative difference (%)
Hogging			
(18.534, 17.500)	20.68	20.643	0.18
(16.789, 16.858)	19.61	19.834	−1.14
(16.205, 16.816)	18.82	19.145	−1.73
(17.452, 16.830)	20.46	20.365	0.46
Sagging			
(18.288, 24.992)	25.07	24.992	0.31
(16.858, 16.789)	23.76	23.728	0.13
(15.983, 16.616)	22.67	22.652	0.079
(17.452, 16.830)	24.41	24.578	−0.69

5.4. Accounting for short-term variability of the response

The environmental contour approach is typically used to give an approximate solution to the full long-term response without the need for a large number of computational heavy response calculations. However, it is important to acknowledge that this is only an approximate method, and it does not properly take the short-term variability of the response in a sea state into account. In situations where the short-term variability of the response is not negligible compared to the long-term variability of the environmental conditions, this may lead to non-conservative results and some corrections may be needed in order to obtain better estimates of the long-term extreme response. This is well known, and in Ref. [42] it is suggested that the effect of short-term variability may be accounted for by either inflating the contours or by inflating the response by replacing the characteristic extreme value of the response in a sea state by a higher percentile of the extreme response distribution, see also [3,49]. The appropriate correction factors will be case-specific and will need to be calibrated in a case-by-case manner. Typically, by inflating the response one may assume a percentile within the range of 75%–90% depending on the structure, the structural responses of interest and the return period.

Also for the response based approach outlined in this paper there may be a need to apply correction factors in order to account for short-term variability of the response. However, this can be done in a similar way as with the environmental contour approach by inflating the response. That is, rather than fitting a response emulator to the characteristic extreme value (eq. (13)) one may rather calculate some higher percentile level of the extreme response distribution and fit the emulator to this level. The p-level percentile of the extreme response distribution can be calculated as,

$$x_p = \gamma + \alpha\left(-\ln\left(1 - p^{\frac{1}{N}}\right)\right)^{\frac{1}{\beta}}. \tag{14}$$

where p denotes the fractile level [42]. Typically, the percentile would be in the range of 75%–90% percentile levels, but the most

appropriate level would be case-specific and should be carefully calibrated in each case. In this way, the short-term variability can be approximately taken into account in order to improve the estimates of the long-term extreme response.

It is out of scope of this case study to carry out a full long-term response analysis for validation and calibration of correction factors, and in this study the short-term variability has been neglected. However, it is important to note that in a real design case, appropriate calibration is needed. This could be done in a similar way for both the contour-based and the response-based approaches, for example by applying a correction factor by inflating the response by a fixed fractile level as outlined above. Notwithstanding, for cases where the short-term variability dominates the long-term variability, such approximate methods should be used with care, and there may be a need for full long-term response analyses. How to do properly account for both long-term and short-term variability using response emulators will be a topic for further research.

6. Summary and conclusions

This paper explores response-based methods for extreme hogging and sagging response analysis of an LNG tanker, utilizing a response emulator based on Gaussian processes regression and compares with contour-based methods. The use of environmental contours for approximate analyses in structural reliability of marine structures is a well-recognized practice in the industry, and also response-based methods based on emulators have recently gain much attention. Hence, such a comparison is relevant to the industry.

The comparison of response-based and contour-based methods reveals that the approaches give comparable results with differences of the same order as differences between different extreme value analysis techniques applied to response time-series with the response-based approach. Hence, both methods can be seen to give reasonable approximations to the extreme response in this case. Also, by comparing the statistical response emulator to results from full hydrodynamical calculations for selected extreme sea states, it is found that the emulator is a good approximator to the numerical model. Nevertheless, uncertainties for extreme response estimation remains large, and in particular, the extrapolation of response data to extreme responses yields large uncertainties - even with quite long time-series corresponding to 30 and 90 years of data.

The sea states giving rise to the 25-year extreme responses have also bee investigated, and it is observed that the estimates from the response-based analysis correspond to sea-states well outside the 25-year environmental contours. This could be construed to mean that the 25-year response could be generated by sea-states with longer return period than 25 years. This may seem counter-intuitive, but could possibly be explained by the small amount of data in the tails of the distribution – even with quite long time-series – and uncertainty due to how well parametric models fitted to the data describe tail behaviour. Such fitting is needed with both approaches, as they form the basis for environmental contours as well as response-based extreme value analysis. Hence, in order to reduce uncertainties, more data would be recommended.

In comparing different environmental contour methods we have considered the effect of different modelling approaches for preprocessing of the environmental variables, i.e. an all sea states approach and a storm peak approach. In the case study presented here, all approaches to contour estimation were found to give reasonable and comparable results. However, it is believed that in more complicated cases, for example with more environmental variables in play, differences between contour methods may become larger. Nevertheless, for the case study presented in this paper, it is difficult to discriminate between the contour methods, and they are all found to perform reasonably well. Further investigations with more complex structural problems are recommended in order to investigate the relative merits of the different contour methods.

Acknowledgement

The work presented in this paper has been carried out within the research project ECSADES, with support from the Research Council of Norway (RCN) under the MARTEC II ERA-NET initiative; project no. 249261/O80.

References

[1] Haver S, Kleiven G. Environmental contour lines for design purposes - why and when? Proc. 23rd international conference on offshore mechanics and arctic engineering (OMAE 2004). American Society of Mechanical Engineers (ASME); 2004.
[2] Haver S. On the joint distribution of heights and periods of sea waves. Ocean Eng 1987;14:359–76.
[3] Winterstein S, Ude T, Cornell C, Bjerager P, Haver S. Environmental parameters for extreme response: inverse FORM with omission factors. Proc. 6th international conference on structural safety and reliability. 1993.
[4] Haver S, Winterstein S. Environmental contour lines: a method for estimating long term extremes by a short term analysis. Trans - Soc Nav Archit Mar Eng 2009;116:116–27.
[5] Huseby AB, Vanem E, Natvig B. A new approach to environmental contours for ocean engineering applications based on direct Monte Carlo simulations. Ocean Eng 2013;60:124–35.
[6] Huseby AB, Vanem E, Natvig B. Alternative environmental contours for structural reliability analysis. Struct Saf 2015;54:32–45.
[7] Vanem E, Bitner-Gregersen EM. Alternative environmental contours for marine structural design - a comparison study. J Offshore Mech Arct Eng 2015;137:1–8. 051601.
[8] Vanem E. A comparison study on the estimation of extreme structural response from different environmental contour methods. Mar Struct 2017;56:137–62.
[9] Huseby AB, Vanem E, Eskeland K. Evaluating properties of environmental contours. Proc. ESREL 2017. European Safety and Reliability Association(ESRA); 2017.
[10] Leira BJ. A comparison of stochastic process models for definition of design contours. Struct Saf 2008;30:493–505.
[11] Haselsteiner AF, Ohlendorf J-H, Wosniok W, Thoben K-D. Deriving environmental contours from highest density regions. Coast Eng 2017;123:42–51.
[12] Silva-González F, Heredia-Zavoni E, Montes-Iturrizaga R. Development of environmental contours using Nataf distribution model. Ocean Eng 2013;58:27–34.
[13] Dahl KR, Huseby AB. Buffered environmental contours. Proc. ESREL 2018. European Safety and Reliability Association(ESRA); 2018.
[14] Li Q, Gao Z, Moan T. Modified environmental contour method for predicting long-term extreme responses of bottom-fixed offshore wind turbines. Mar Struct 2016;48:15–32.

[15] Montes-Iturrizaga R, Heredia-Zavoni E. Environmental contours using copulas. Appl Ocean Res 2015;52:125–39.
[16] Chai W, Leira BJ. Environmental contours based on inverse SORM. Mar Struct 2018;60:34–51.
[17] Manuel L, Nguyen PT, Canning J, Coe RG, Eckert-Gallup AC, Martin N. Alternative approaches to develop environmental contours from metocean data. J Ocean Eng Mar Energy 2018;4:293–310.
[18] Ross E, Astrup OC, Bitner-Gregersen E, Bunn N, Feld G, Gouldby B, Huseby A, Liu Y, Randell D, Vanem E, Jonathan P. On environmental contours for marine and coastal design. Ocean Engineering in press; 2019.
[19] Wang S, Wang X, Woo WL. A comparison of response-based analysis and environmental contour methods for FPSO green water assessment. Proc. 37th international conference on ocean, offshore and arctic engineering (OMAE 2018). American Society of Mechanical Engineers (ASME); 2018.
[20] Vanem E, Bingjie G. Comparison of the environmental contour method and response-based analysis using response emulator for estimating extreme ship responses. Proc. 38th international conference on ocean, offshore and arctic engineering (OMAE 2019). American Society of Mechanical Engineers (ASME); 2019.
[21] Huseby AB, Vanem E, Natvig B. A new Monte Carlo method for environmental contour estimation. Proc. ESREL 2014. European Safety and Reliability Association(ESRA); 2014.
[22] Vanem E. 3-dimensional environmental contours based on a direct sampling method for structural reliability analysis of ships and offshore structures. Ships Offshore Struct 2018;14:74–85.
[23] Jonathan P, Ewans K, Flynn J. On the estimation of ocean engineering design contours. J Offshore Mech Arct Eng 2014;136:1–8. 041101.
[24] Vanem E. Joint statistical models for significant wave height and wave period in a changing climate. Mar Struct 2016;49:180–205.
[25] Vanem E. Uncertainties in extreme value modeling of wave data in a climate change perspective. J Ocean Eng Mar Energy 2015;1:339–59.
[26] Gramstad O, Vanem E, Bitner-Gregersen E. A simulation study on the uncertainty of environmental contours due to sampling variability for different estimation methods" (2019), Erik Vanem, Odin Gramstad, Elzbieta M. Bitner-Gregersen. Appl Ocean Res 2019;91:101870.
[27] Montes-Iturrizaga R, Heredia-Zavoni E. Assessment of uncertainty in environmental contours due to parametric uncertainty in models of the dependence structure between metocean variables. Appl Ocean Res 2017;64:86–104.
[28] Silva-González F, Vázques-Hernández, Sagrilo L, Cuamatzi R. The effect of some uncertainties associated to the environmental contour lines definition on the extreme response of an FPSO under hurricane conditions. Appl Ocean Res 2015;53:190–9.
[29] Williams CK, Rasmussen CE. Gaussian processes for regression. Touretzky Ds., Mozer Mc., Hasselmo ME, editors. Advances in neural information processing systems, vol. 8. MIT Press; 1996.
[30] Aarnes OJ, Reistad M, Breivik Ø, Bitner-Gregersen E, Eide LI, Gramstad O, Magnusson AK, Natvig B, Vanem E. Projected changes in significant wave height towards the end of the 21st century - northeast Atlantic. J Geophys Res: Oceans 2017;122:3394–403.
[31] Bitner-Gregersen EM, Vanem E, Gramstad O, Hørte T, Aarnes Oj, Reistad M, Breivik Ø, Magnussen AK, Natvig B. Climate change and safe design of ship structures. Ocean Eng 2018;149:226–37.
[32] Bitner-Gregersen EM. Joint met-ocean description for design and operation of marine structures. Appl Ocean Res 2015;51:279–92.
[33] Ewans K, Jonathan P. The effect of directionality on northern North Sea extreme wave design criteria. J Offshore Mech Arct Eng 2008;130:1–8. 041604.
[34] Heffernan JE, Tawn JA. A conditional approach for multivariate extreme values. J R Stat Soc Ser B 2004;66:497–546.
[35] Ross E, Sam S, Randell D, Feld G, Jonathan P. Estimating surge in extreme North Sea storms. Ocean Eng 2018;154:430–44.
[36] Randell D, Turnbull K, Ewans K, Jonathan P. Bayesian inference for nonstationary marginal extremes. Environmetrics 2016;27:439–50.
[37] IACS. Common structural rules for bulk carriers and oil tankers. 2019.
[38] Naess A, Moan T. Stochastic dynamics of marine structures. Cambridge University Press; 2012.
[39] Dommermuth DG, Yue DKP. A high-order spectral method for the study of nonlinear gravity waves. J Fluid Mech 1987;184:267–88.
[40] West BJ, Brueckner KA, Janda RS, Milder DM, Milton RL. Anew numerical method for surface hydrodynamics. J Geophys Res - Oceans 1987;92:11803–24.
[41] Guo B, Bitner-Gregersen EM, Sun H, Helmers JB. Statistical analysis of ship response in extreme seas. Ocean Eng 2016;119:154–64.
[42] DNV GL. Environmental conditions and environmental loads. DNV GL; 2017. DNVGL-RP-C205.
[43] Baarholm GS, Moan T. Estimation of nonlinear long-term extremes of hull girder loads in ships. Mar Struct 2000;13:495–516.
[44] Bateman W, Swan C, Taylor P. On the calculation of the water particle kinematics arising in a directionally spread wavefield. J Comput Phys 2003;186:70–92.
[45] Guo B, Gramstad O, Vanem E, Bitner-Gregersen E. Study on the effect of climate changes on ship responses based on nonlinear simulations. J Offshore Mech Arct Eng 2019;141:1–13. 041605.
[46] Ewans K, Jonathan P. Evaluating environmental joint extremes for the offshore industry using the conditional extremes model. J Mar Syst 2014;130:124–30.
[47] Randell D, Feld G, Ewans K, Jonathan P. Distributions of return values for the ocean wave characteristics in the South China Sea using directional-seasonal extreme value analysis. Environmetrics 2015;26:442–50.
[49] Winterstein SR, Engebretsen K. Reliability-based prediction of design loads and responses for floating structures. Proc. 17th international conference on offshore mechanics and arctic engineering (OMAE 1998). American Society of Mechanical Engineers (ASME); 1998.